World Journal of Environmental Biosciences
Available Online at: **www.environmentaljournals.org**

Volume 14, Issue 2: 107-118

https://doi.org/10.51847/Rd8ub5wo3G

ISSN 2277- 8047

Assessment of Potential Surface Runoff in Tulasi Watershed of Kolhapur Using NRSC-CN Method

Vikramsinh Subhashrao Pawar-Patil[1], Abdulwahhab Jasim Mahdi[2], Ashish Vilas Mane[3]*, Sachin Shantaram Panhalkar[4], Sambhaji Dnyaneshwar Shinde[4], Sainath Aher[5]

[1]Department of Geography, The New College, Kolhapur 416012, Maharashtra, India.
[2]Department of Environmental Pollution, College of Environmental Sciences, Al-Qasim Green University, Babylon 51013, Iraq.
[3]Department of Environmental Science, Fergusson College (Autonomous), Savitribai Phule Pune University, Pune 411004, Maharashtra, India.
[4]Department of Geography, Shivaji University, Kolhapur 416004, Maharashtra, India.
[5]Universal Geotechnica, Nashik 422011, Maharashtra, India.

ABSTRACT

Indian watersheds form an important part of the contiguous water resources , particularly in the changed environments, which leads to urbanization and affects the climatic pattern. A concern of sustainable watershed management relates to the runoff assessment, as excessive runoff can cause flooding, while insufficient runoff can lead to water scarcity. In the current work, model has taken a typical TULASI watershed in the Kolhapur (Maharashtra) mountain range, and the approach is based on the National Remote Sensing Centre Curve Number (NRSC-CN) methodology. This data set was exported to the Soil and Water Assessment Tool (SWAT) using the ArcGIS extension and then re-projected from the elevation figures in coordinate system UTM North zone 43 using the Spatial reference transformation framework. The Tulasi watershed, with its seven sub-watersheds, was delimited in the same software platform with points of discharge defined. General evaluation of the NRCS-CN model revealed that a medium runoff depth, about 729 mm, is common for small catchments, whereas maximum values of surface runoff were observed during the monsoon in 2013, the twenty-first year of the studied period. Elevated and very elevated runoff potentials were observed in hilly lands and in most parts of the sloping areas under central and the lower reaches of sub-watersheds. The interpretation shows the general occurrences of potential surface runoff to be predominantly medium among the watersheds investigated; however, the occurrences tend to occur in upper reaches, which have a dense forest coverage and a coarse-textured surface of the soil.

Keywords: *Surface runoff, Tulasi watershed, NRSC-CN method, Geographic information system (GIS), Global positioning system*

Corresponding author: Ashish Vilas Mane
e-mail ✉ ashish.mane@fergusson.edu
Received: 02 March 2025
Accepted: 21 July 2025

INTRODUCTION

Incorporation of micro-level natural resource planning into the conservation structures aimed to control the unregulated surface water, thus controlling the soil water degradation (Dharmawan *et al*., 2023). For power generation, water supply, and flood control, the importance of quantifiable watershed runoff and its magnitude can be particularly noted when considering flood prediction (Jehanzaib *et al*., 2022; Kumar *et al*., 2023; Jahanbani *et al*., 2024). Hence, in terms of the water cycle, precipitation and water runoff together with the associated connected networks contribute to the formation of the watershed Mondal and Mishra, (2024). Superficial processes happen only when intensive rainfall is more than the infiltration capacity (Allan *et al*., 2021). Pareta and Pareta (2012) and Bhardwaj (2019) describe that at least the rainfall should be able to compensate evapotranspiration, interception, infiltration, and surface storage to the advantage of surface runoff. Surface water movement becomes largely dispersed when rainfall intensity surpasses the soil infiltration capacity (Xu *et al*., 2024).

The term surface detention refers to water temporarily retained in depressions or gullies, whereas channel detention indicates water stored within stream channels. Both surface and channel detention, together with groundwater baseflow recharge, contribute to subsurface water storage (Fan *et al*., 2024). Additionally, flow may exhibit a lateral component, facilitating water movement into subterranean stream networks. The interactions governed by groundwater flow control not only the recharge process but also the dynamic coupling between surface water and groundwater systems (Coppol *et al*., 2022; Banerjee & Ganguly, 2023; Ma *et al*., 2024; Prada *et al*., 2024).

The Geoinormative Integrated Model (GNIM) addresses key parameters in precipitation planning and hydrological monitoring to enhance traditional runoff models. By incorporating land use–land cover, hydrological soil group, and precipitation distribution, GNIM enables the generation of these variables with high accuracy. The approach leverages geospatial

technologies to manage spatial processes across large regions efficiently, improving model performance and reliability compared to conventional methods (Baghel, 2023; Saber *et al*., 2023; Doost *et al.*, 2024).

MATERIALS AND METHODS

Curve number assessment technique of runoff assessment by soil conservation service

Surface as well as the base flow are the main elements of streamflow that can be distinguished individually by mathematical models; however, geoinformatics (GIS) is essential in considering the evaluation of runoff (Kalogeropoulos *et al.*, 2020). The rain precipitation runoff surface interaction is recognized as a component of the complex nonlinear processes that characterize the real world in hydrological engineering (Jehanzaib *et al*., 2022). Numerous hydrological models have been designed with the aim to predict maximum runoff that results from intense precipitation. Nevertheless, it has been discovered that that most modelling approaches require a lot of data, require extensive calibration, and cannot be used in non-field settings (Kratzert *et al*., 2024). One illustration of this restriction is the Natural Resources Conservation Service Curve Number (NRCS-CN) model.

The Soil Conservation Service Curve Number (SCS-CN), also known as the Soil Conservation Service Probability Model, is an evaluation method developed after the fact by the United States Department of Agriculture (Soil Conservation Service, 1972) and used to evaluate surface runoff. The selected modelling approach considers runoff creation as well as watershed variables that influence runoff, particularly land cover and utilization, soil hydrological features, and soil moisture levels prior to the droplet creating a flow in a stream channel (Auerswald & Gu, 2021).

NRCS-CN is based on the principles of water balance and two assumptions (Soil Conservation Service, 1972). The first one, where a given ratio between the quantity of the runoff generated on a surface (Q) of susceptible soil during a period of precipitation and the total precipitation (P) was considered constant. The second assumption is that the upper acceptable limit of the retention that is likely to be (Ia) is known. Thus, the SCS-CN method is modeled by the following equation.

$$P = Ia + F + Q \quad (1)$$

where P represents total rainfall (mm), Ia represents initial abstraction (mm), F represents collective infiltration (mm) and Q represents direct runoff (mm).

The loss, e.g., in interception, surface storage, and infiltration, has to be taken into account by the initial abstraction (Ia) before precipitate volume is transformed into runoff (Pareta & Pareta, 2012). Another assumption is that there is a direct relationship between total rainfall (P) and direct runoff (Q) as well as between initial loss (Ia) and storage capacity (S), which may be represented respectively

$$Q / (P - Ia) = F / S \quad (2)$$

where S is watershed capacity of recharge for 5 days (antecedent and precipitation over the next 5 days).

The notion of first abstraction (Ia) is supposed to be the part of the maximum retention (S).

$$Ia = \alpha S \quad (3)$$

Where a = the preliminary abstraction ratio.

The original SCS-CN way adopts that alpha = 0.2 for practical use. Empirical studies done in the USA and elsewhere (Soil Conservation Service, 1972, SCD, 1972) have shown that al is normally between 0 and 0.3. Doing the math described in Eqs. 1 through 3 gives a new expression for Q as:

$$Q = [(P - Ia)^2] / [(P - Ia) + S] \quad (4)$$

Eq. 4 is applicable if P>Ia; otherwise Q=0. All the relationships expressed in Eqs. 1 through 4 are depth or capacity based.

The S parameter, SCS-CD, in the SCS-CN method depends on the land use/land cover, soil type, hydrology status, and antecedent moisture state (AMS). Therefore, as a non-parameterized model for the surface runoff from the daily precipitation of an annual extreme rainfall event, the SCS-CN model having a value of a = 0.2 can be used, which was originally obtained from daily rainfall-runoff data (Rallison, 1980). In light of the variation of values that may be assumed by the parameter S, it may be transformed into another curve number (CN) that may assume values in the more traditional range of 0 - 100:

$$S = (25400 / CN - 254) \quad (5)$$

S = CN, where the Curve Number is expressed in millimetres. The only main difference between S and CN is that the former is a non-dimensional value, whereas the latter is the dimensional value. The prescribed range of CN is 0 – 100, and empirically valid design standards are between 40 and 98 (Van, 1989). The Curve Number that is attributed to hydrological soil cover is dependent on soil type, land cover, and one of three antecedent soil moisture conditions (AMC I, AMC II, and AMC III).

Moisture conditions at the time of incident

The SCS procedure utilizes Antecedent Soil Moisture Condition (AMC) classification to represent moisture condition prior to a rainfall event for rainfall abstraction modeling. AMC I denotes dry soil conditions with low moisture content, where cumulative rainfall over the preceding five days is less than 12.5 mm during the dormant season or below 35 mm in the growing season. AMC II reflects average soil moisture, occurring when the five-day antecedent rainfall ranges between 12.5 and 27.5 mm in the dormant season or between 35 and 52.5 mm during the growing season. AMC III corresponds to wet soil conditions, characterized by high moisture saturation, where rainfall over the previous five days exceeds 27.5 mm in the dormant season or 52.5 mm in the growing season.

Database preparation

The CN coefficient, also considered as the watershed coefficient, is an index that includes the Hydrological Soil Group (HSG) classification and land-cover type, both of which are required for CN calculation (Chow *et al*., 1988; Mishra *et al*., 2006; Nag *et al*., 2022, Kaliraj *et al*., 2023). First, an SRTM-DEM raster having a spatial determination of 30 m was analyzed in the ArcGIS 9.3 environment to find the position of the major watershed and

sub-watersheds in the main watershed. The elevation data was projected to the UTM 43N coordinate system using the Spatial reference transformation framework before being transmitted using SWAT software's ArcGIS extension. This software modeling tool was used to delineate seven sub watersheds of the Tulasi watershed, as well as identify the outlet point for sub watershed.

LULC mapping

The assessment of surface overflow based on well-defined LULC classification and subsequent foot printing for their accurate estimation is used for the NRCS-CN model (Kumar *et al*., 2022). The LULC map was constructed using a hybrid classification technique with the assistance of Google Earth Pro imagery and satellite imagery of the study area with the LISS-III sensor (23.5 m) and Google Earth Pro imagery (10 m). Prior to statistical analyses prior to preprocessing of the LISS-III data by means of ERDAS Imagine version 9.2 was conducted employing a supervised classification algorithm. The resulting classified co-axis scatter photogrammetry map was then added to the ArcGIS workspace, where it was compared with a toposheet and Google Earth imagery of the watershed. This visual classification was further confirmed by means of abundant field observations, and this resulted in a strong LULC map (da Silva *et al*., 2020).

HSG map preparation

The soil texture map of Kolhapur district (provided by the National Soil Survey and Land Use Planning (NBSS and LUP) Nagpur (2005)) was used for preparing the HSG map for the watershed **(Figure 2)**, considering the requirement of soil texture in watershed hydraulics. Surface-soil data on soil textures were used to quantify the extents of sand, silt, and clay soil fraction of the surface soils using soil-mapping information in the Surface Observations and Soil Texture Estimation Resource (SOTER) database. Empirical methodologies were also adopted to identify the soil texture position with different elevations within the watershed, with the finalized HSG map **(Figure 2)**.

CN II map preparation

Thematic overlay of the LULC and HSG layers was performed in ArcGIS to calculate the CN II values across the watershed. Correlation to Normalization (CNII) values were determined using standardized tables (SCS 1972 and other reference materials such as Mishra *et al*. (2006) and Tideman (2000). A weighted CNII (WCN) was calculated. The computed CN II values were then adjusted for slope effects, as the classic SCS-CN model does not account for the rising effect of topography on indicating runoff, resulting in reduced surface flow rates **(Table 1)**. When combining slope parameters, use gradient-based adjustment according to the methods given by Haung *et al*. (2006), where slope is explicitly engaged in the CN computation.

$$\text{CN II}\boldsymbol{\alpha} = \text{CN II}\frac{322.79 + (15.63) * \alpha}{\alpha + 323.52} \quad (6)$$

Where,

CN II**α =** Slope Corrected CN value

CN II = WCN of CN II value

α = Slope (m m^{-1}) ranges 14% to 140%

Eq. 6 through an ArcGIS spatial algorithm - the surface-slope tool - was used to calculate the surface gradient and the run-off slope in terms of octree percent increase. These parameters have been used as inputs to the raster-based calculation of this index, the slope-adjusted CN II value, for the watershed **(Figure 4)**. The zonal statistic is assumed to be equivalent to the mean values of CN IIa of all sub watersheds within the ArcGIS framework (Eniyew *et al*., 2024).

The dry and wet curve numbers was taken from three original studies by Sobhani (1975), Hawkins *et al*. (1985), Chow *et al*. (1988), and Neitsch *et al*. (2000). Out of these, the Sobhani *et al*. (1975) and Hawkins *et al*. (1985) formulations were found to have the best potential to get the CN I and CN III values, correspondingly (Mishra *et al*., 2008).

$$\text{CN} - \text{I} = \frac{\text{CN(II)}}{2.334 - 0.01334 * \text{CN(II)}} \quad (7)$$

Sobhani (1975)

$$\text{CN III} = \frac{\text{CN II}}{0.427 + 0.00573 * \text{CN II}} \quad (8)$$

Hawkins *et al*. (1985)

Direct runoff (Q) assessment

Then with Eq. 5 and with the values of CN IIa along with the respective values of CN I and CN III, the factor Ss (mm) of each of the sub watersheds has been determined as follows. The initial abstraction (Ia) has been derived in the following equation.

$$\text{Ia} = \text{I S} \quad (9)$$

The majority of worldwide studies presuppose that l equals 0.2, however, empirically derived relationships are the part that would be taken into account in the computation of Ia considering Indian circumstances, given that Fallows were applied in the current research **(Table 1)**.

The equations of black soil region AMC II and III: I a = 0.1S

Black Soil Region AMC I: Ia = 0.3*S

Rainfall data on which the AMC data have been computed have been given by the Global Weather Data. Due to the data on the daily rainfall of the year 2013, the data was imported by using the Excel software and the AMC, AMC-class, and S=Potential maximum Retention or Forigination, after which the Sections, being Q=Direct runoff as well as the Ia=Initial abstraction, were calculated using the respective equations with the help of the said calculations.

RESULTS AND DISCUSSION

Land use/ Land cover map

Though the flowing rainwater is not actually reducing the number of habitats, it is the emphasis that should be placed on the land-based factors (Sahavacharin *et al*., 2022). Recently land has been defrauded and cleared, or the magnitude changes are a result of natural and anthropogenic landscape changes that hinder and balance the external precipitation of water **(Figure 1)**. The high watershed regions, particularly the west

slopes of the declivous hilly topography, are forested with mixed trees and open scrub, while the mid-course areas and lower portions are mostly barren. The cultivation of sugarcane is concentrated in lowland zones of the downstream drainage system, where rice and ragi, grown during the rainy period, are mostly established on slopes and hillsides susceptible to the existence of slips.

The distribution of land use and land cover in the study area indicates that agriculture is the dominant category, occupying 76.03 km^2, which represents 46.50% of the total geographical area. Barren land covers 25.80 km^2 (15.78%), followed by open scrub extending over 20.16 km^2 (12.33%) and fallow land occupying 15.70 km^2 (9.60%). Forest-related classes together occupy a smaller proportion of the area, with forest cover accounting for 8.49 km^2 (5.19%), open mixed forest covering 3.91 km^2 (2.39%), and medium scrub with scattered trees extending over 1.43 km^2 (0.87%). Settlements occupy 4.24 km^2 (2.59%), while rivers and other water bodies together cover 7.75 km^2, constituting 4.74% of the whole area. The overall area considered in this study is 163.51 km^2 **(Figure 1)**.

Soil texture and the complexity of soil hydrology cover.

It is depending on water availability absorbed by bare soil, which pertains to the distinction of four categories of hydrologic soil (Li *et al*., 2021; Feldman *et al*., 2024; Vereecken *et al*., 2024) The significance of hydrology and water resources in tropical islands has received increased attention of late (Sánchez-Murillo *et al*., 2020). The soil groups created by the U.S. Natural Resource Conservation Service (NRCS) are characterized on the basis of their hydrologic characteristics with 4 distinct DNS groups based upon their infiltration rates (NRCS, 1996). A hydrologic group consists of soils that have a similar runoff potential under similar storm conditions. Soils characteristics that affect natural drainage capacity include depth to watertable, saturated hydraulic conductivity and depth to unsaturated layers (Yang *et al*., 2020). In the Tulasi watershed, soils are classified under the A, B, C, and D categories, ranging from clay and silty clay to sandy and coarse sandy soils. The hydrological soil cover complex of the study area shows that sandy clay loam soils classified under Hydrological Soil Group (HSG) B are the most extensive, covering 52.10 km^2 or 31.87% of the total area. Coarse sandy loam soils belonging to HSG A occupy 41.98 km^2 (25.68%), followed by clay loam soils under HSG D covering 37.30 km^2 (22.81%). Silty clay loam soils classified as HSG C extend over 32.13 km^2, accounting for 19.65% of the study area. In this study, the land use–land cover distribution and soil hydrological classification classification were computed using classified satellite imagery representing the study area along with the soil texture map **(Figure 2)**.

Table 1. Computed CN II values for the Tulasi Watershed

Soil Texture	HSG	LU/LC Class Name	Area (Sq. km.)	CN_II	CN II*Area
Sandy Clay Loam	B	**Barren Land**	5.399	85.000	458.955
Sandy Clay Loam	B	**Agriculture**	21.763	81.000	1762.795
Sandy Clay Loam	B	**Fallow Land**	4.165	86.000	358.205
Sandy Clay Loam	B	**Forest**	8.257	50.000	412.831
Sandy Clay Loam	B	**Open Mixed Forest**	2.708	66.000	178.741
Sandy Clay Loam	B	**Open Scrub**	9.049	47.000	425.317
Sandy Clay Loam	B	**Settlement**	0.446	85.000	37.906
Clay Loam	D	**Barren Land**	2.758	91.000	250.956
Clay Loam	D	**Agriculture**	27.616	91.000	2513.020
Clay Loam	D	**Fallow Land**	3.738	94.000	351.349
Clay Loam	D	**Water Bodies**	0.115	100.000	11.531
Clay Loam	D	**Forest**	0.013	77.000	0.990
Clay Loam	D	**Settlement**	1.244	92.000	114.477
Clay Loam	D	**River**	1.723	100.000	172.270
Sandy Clay Loam	B	**Water Bodies**	0.333	100.000	33.271
Sandy Clay Loam	B	**Medium Scrub and Trees**	0.003	66.000	0.224
Coarse Sandy Loam	A	**Barren Land**	12.128	76.000	921.743
Coarse Sandy Loam	A	**Agriculture**	11.131	72.000	801.454
Coarse Sandy Loam	A	**Fallow Land**	4.016	77.000	309.200
Coarse Sandy Loam	A	**Forest**	0.226	25.000	5.645
Coarse Sandy Loam	A	**Open Mixed Forest**	1.315	45.000	59.159
Coarse Sandy Loam	A	**Water Bodies**	0.100	100.000	9.951
Coarse Sandy Loam	A	**Medium Scrub and Trees**	1.424	45.000	64.062

Coarse Sandy Loam	A	**Open Scrub**	9.896	33.000	326.568
Coarse Sandy Loam	A	**Settlement**	1.822	77.000	140.312
Silty Clay Loam	C	**Barren Land**	5.580	89.000	496.632
Silty Clay Loam	C	**Agriculture**	15.319	88.000	1348.081
Silty Clay Loam	C	**Fallow Land**	3.706	86.000	318.697
Silty Clay Loam	C	**Water Bodies**	5.221	100.000	522.141
Silty Clay Loam	C	**Forest**	0.084	70.000	5.894
Silty Clay Loam	C	**Open Scrub**	1.215	64.000	77.784
Silty Clay Loam	C	**Settlement**	0.770	90.000	69.293
Silty Clay Loam	C	**River**	0.226	100.000	22.597
			163.509		12582.049

Source: Assigned curve number II for different land parcels of lu/lc covered by HSG is crudely obtained from standard tables of SCS (1972); Chow *et al*. (1988); Tideman (2000) and Mishra *et al*. (2006).

Weighted CN II (WCN)= (CN II * Area/Total Watershed Area)

Where, CN II* Area (km^2) = **12582.049**

Total Watershed Area (km^2) =**163.509 km^2**

Hence, **WCN II = 76.95**

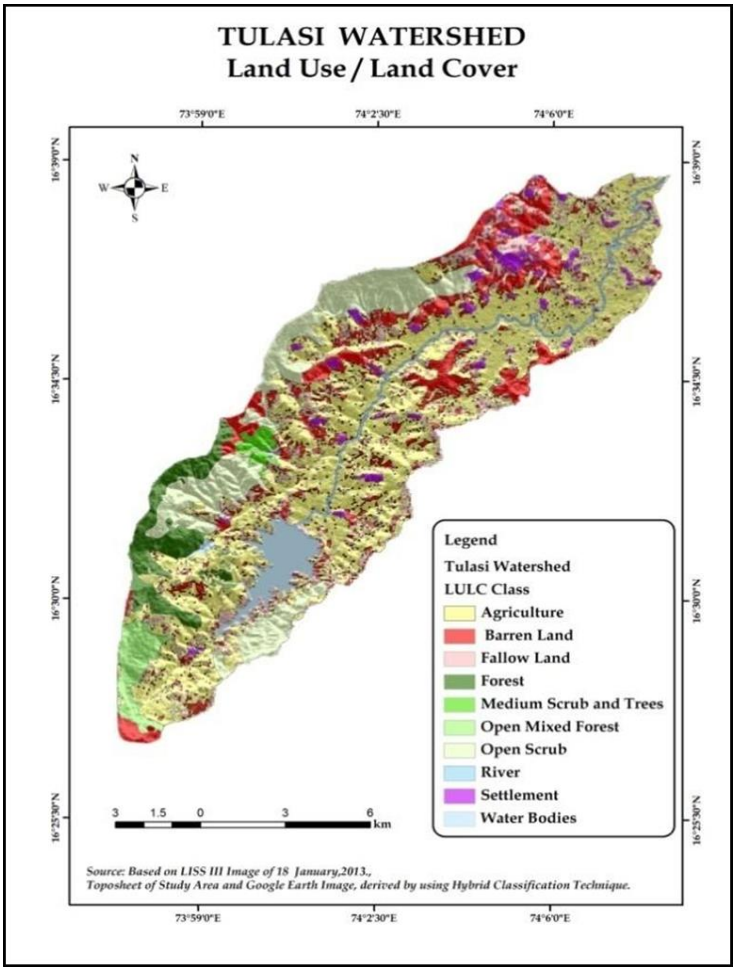

Figure 1. Land Use/Land Cover Map

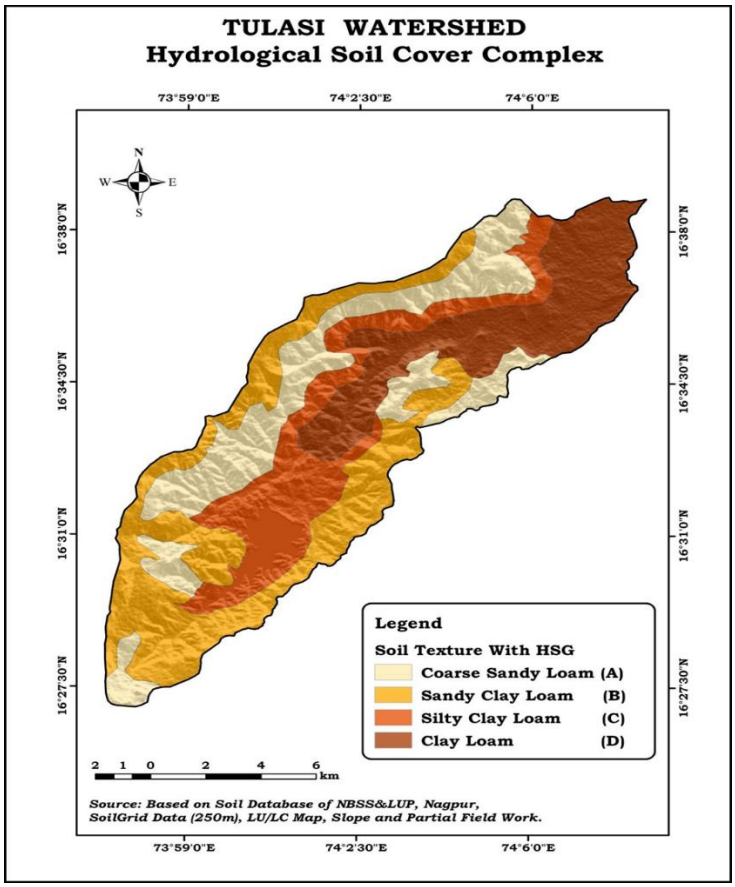

Figure 2. Soil Texture Map

Section of requisite for computing slope-corrected Curve Number II (CN2) **(Table 1)**. Using the tabulated data, weighted CN II was found for the total watershed of Tulasi to be 76.95. The derived CN 2 raster layer, along with the percent slope of the study watershed **(Figure 3)**, was processed in the ArcGIS environment to produce a slope-corrected CN 2 map **(Figure 4)**. This raster representation assigns representative values of CN II to each sub watershed, and, sub watershed by sub watershed, values of CN I and CN III (as slope corrected) were also evaluated **(Table 1)**.

The distribution of slope-corrected Curve Number (CN) values across the Tulasi watershed shows clear variation among sub-watersheds under different antecedent moisture conditions. In sub-watershed TS-1, the slope-corrected CN values increase from 54.21 under AMC I to 73.43 under AMC II and further to 86.62 under AMC III. TS-2 exhibits comparatively lower runoff potential, with CN values of 39.42, 60.30, and 78.06 for AMC I, AMC II, and AMC III, respectively. Higher CN values are observed in TS-3 and TS-4, where TS-3 records 66.76, 82.42, and 91.65, while TS-4 shows 68.66, 83.64, and 92.29 as soil moisture conditions progress from dry to wet **(Figure 4)**.

In TS-5, the slope-corrected CN values rise from 52.74 during AMC I to 72.26 during AMC II and 85.92 during AMC III. A similar increasing trend is evident in TS-6, with CN values of 63.84, 80.47, and 90.61. TS-7 displays the highest runoff potential among all sub-watersheds, with slope-corrected CN values of 75.22 for AMC I, 87.63 for AMC II, and 94.32 for AMC III. When considered at the watershed scale, the Tulasi watershed shows average slope-corrected CN values of 58.86 under AMC I, 76.96 under AMC II, and 88.66 under AMC III. In this study, the slope-corrected CN values were obtained through a GIS-based analytical approach **(Figure 4)**.

These CN values mostly show a stochastic distribution with higher values in the lower reaches that are contributed by the predominance of the forested area and the sandiness of the areas in the upper sections of the Tulasi watershed. The presence of fine-grain clay patches and steep, shallow land along riverbeds on both elevations within the ridges makes elevation retention of elevated CN values in the lower watershed easy. Consistent with this, Zhang *et al*. (2022) examined the impact of the soil's thickness on karst hillslope runoff and rainfall infiltration during storm events.

Rainfall and runoff depth (mm) in tulasi watershed

It has been shown that the runoff per mm per unit rainfall in each sub-watershed, is equal to the depth of runoff derived from the uniform distribution of precipitation over the whole of the Tulasi watershed. The distribution of direct runoff across the Tulasi sub-watersheds under uniform rainfall conditions shows a clear seasonal and spatial variation. During the dry months from January to May, rainfall is very low and no direct runoff is generated in any of the sub-watersheds. With the onset of the monsoon in June, a substantial increase in runoff is observed, with TS-7 recording the highest runoff of 258.2 mm, followed by TS-4 (197.0 mm) and TS-3 (181.2 mm), while TS-2 shows

comparatively lower runoff of 74.51 mm. July produces the maximum runoff across all sub-watersheds due to the highest rainfall, with TS-7 again exhibiting the largest runoff depth of 471.9 mm, followed by TS-4 (386.9 mm) and TS-3 (363.5 mm) (**Table 2 and Figure 5)**.

In August and September, runoff remains significant across all sub-watersheds, with TS-7 consistently showing higher values of 227.3 mm and 280.5 mm, respectively, indicating greater runoff potential. Moderate runoff is observed during October as rainfall decreases, with values ranging from 23.92 mm in TS-2 to 93.36 mm in TS-7. In the post-monsoon months of November and December, rainfall is minimal and generates only negligible runoff, mainly observed in TS-1, TS-3, TS-4, and TS-7. On an annual basis, TS-7 contributes the highest total direct runoff of 1333 mm, followed by TS-4 (1067 mm) and TS-3 (996.8 mm), while TS-2 records the lowest runoff of 415.8 mm. In this study, sub-watershed-wise The computation of direct runoff was carried out using the NRCS–Curve Number method under uniform rainfall conditions.

The Tulasi watershed has an unequal distribution of rainfall since the average rainfall in the basin is said to be lower along the southwest-to-northeast gradient, particularly from the Tulasi River's origin to its confluence. The average rainfall (measured in millimeters) for each sub-watershed has also been calculated and represented in a GIS as part of the data analysis. Additionally, **Table 2** calculates and shows the corresponding runoff depth for the sub-watershed in terms of rainfall. This implies that in the sub-watershed of TS-6, higher runoff depths are modeled in the lower watershed reaches and, conversely, lower runoff in the upland reaches. These results are in agreement with Muppavarapu (2023) and others' case studies on stormwater governance and land use in Jefferson County. There is a strong association between runoff depth and rainfall because rainfall intensity significantly increases runoff within the watershed. Other numerical analyses include crediting the spatiotemporal nature of an event-specific runoff response function in the Lake Erie Basin (Ali *et al*., 2024; Zhou *et al*., 2024), as well as assessing the degree of impact of different rainfall patterns and their interactions on soil and water losses in a small watershed in low hilly terrain. Runoff incidents are expected to be reported more during the wet season, notably from June to October. The optimal runoff condition is for the TS-7 sub-watershed, which comes before TS-4 and TS-3. In the Tulasi watershed, rainfall and runoff fall mostly in July.

The computation of direct runoff was carried out for three sub-watersheds using modified rainfall values and the NRCS–CN approach (**Table 2 and Figure 5)**. The results indicate a strong seasonal dependence of runoff generation. During the dry period from January to May, rainfall remains very low and no direct runoff is produced in any sub-watershed, reflecting high initial losses and unsaturated soil conditions. This phase is dominated by infiltration and storage rather than surface flow.

Table 2. Sub watershed Wise Direct Runoff (Q) Considering Sub-watershed wise Rainfall (mm)

	Sub watershed wise modified rainfall (mm) and runoff (mm)							
	TS-1		TS-2		TS-3		TS-4	
Months	Rainfall (mm)	Runoff (mm)	Rainfall (mm)	Runoff (mm)	Rainfall (mm)	Runoff (mm)	Rainfall (mm)	Runoff (mm)
January	0.015	0	0.015	0	0.014	0	0.013	0
February	4.777	0	4.661	0	4.510	0	4.234	0
March	0.108	0	0.105	0	0.102	0	0.095	0
April	0.063	0	0.061	0	0.059	0	0.056	0
May	18.233	0	17.789	0	17.213	0	16.16	0
June	602.432	136.36	587.767	70.094	568.726	164.90	533.96	168.36
July	823.961	277.86	803.903	140.0	777.861	330.84	730.31	330.62
August	495.002	125.79	482.952	55.85	467.307	149.96	438.742	151.86
September	517.312	175.28	504.719	102.72	488.369	201.01	458.517	199.50
October	237.735	50.830	231.948	22.497	224.434	60.122	210.715	61.156
November	19.121	0.440	18.656	0	18.052	0.479	16.94	0.5797
December	7.620	0.034	7.435	0	7.194	0.0091	6.754	0.0299
Total	2726.380	766.60	2660.010	391.178	2573.840	907.33	2416.51	912.11

Source: Calculated by researcher based on NRCS-CN Method

A clear shift in hydrological response occurs with the onset of the monsoon in June (Li *et al*., 2022). Significant rainfall in June initiates measurable surface runoff, which rises sharply in July and remains elevated through August and September, marking the principal runoff-generating period of the year. Under similar rainfall conditions, sub-watershed TS-7 consistently produces the highest runoff, followed by TS-6, whereas TS-5 exhibits the lowest runoff response. This variation reflects differences in land cover, soil infiltration capacity, and curve number values among the sub-watersheds.

Following September, runoff decreases rapidly as rainfall diminishes (Cao *et al*., 2024). October contributes moderate runoff, while November and December produce only minimal runoff despite light rainfall, suggesting partial replenishment of soil moisture and greater losses due to abstractions. Over the course of the year, cumulative runoff shows considerable variation among the sub-watersheds, with TS-7 contributing the largest portion and TS-5 the smallest. These observations

highlight pronounced spatial variability in runoff behaviour and underline the importance of sub-watershed-specific hydrological analysis for accurate water resource assessment (Ross *et al*., 2024)

The mean monthly rainfall and corresponding runoff potential of the Tulasi watershed exhibit pronounced seasonal variation, accompanied by runoff largely confined to the monsoon period. Very low rainfall is observed in the Tulasi watershed from January to April, ranging from 0.015 mm in January to 0.065 mm in April, during which no surface runoff is generated. In May, rainfall rises to 18.91 mm, yet runoff remains negligible. With the onset of the monsoon in June, rainfall sharply increases to 624.79 mm, producing a runoff depth of 123.02 mm. July experiences the highest precipitation at 854.54 mm, corresponding to the maximum runoff depth of 271.18 mm. Rainfall in August and September measures 513.37 mm and 536.51 mm, resulting in runoff depths of 116.41 mm and 172.25 mm, respectively. Post-monsoon rainfall in October declines to 246.56 mm, generating 46.14 mm of runoff, while November receives only 19.83 mm of rain with minimal runoff of 0.10 mm. December records 7.90 mm of rainfall without any measurable runoff. In total, the watershed accumulates 2827.58 mm of annual rainfall, producing a cumulative runoff of 729.11 mm. In the present study, the monthly surface runoff potential was quantified using the NRCS–Curve Number (CN) method based on the characteristics of the study area.

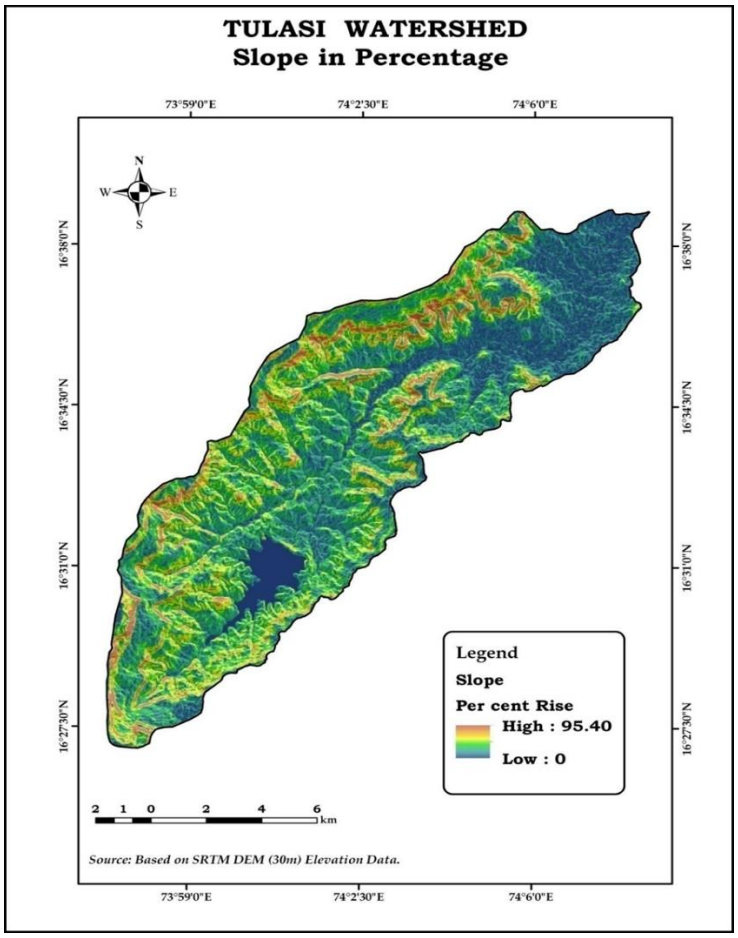

Figure 3. Percent Rise Slope Map of Study Area.

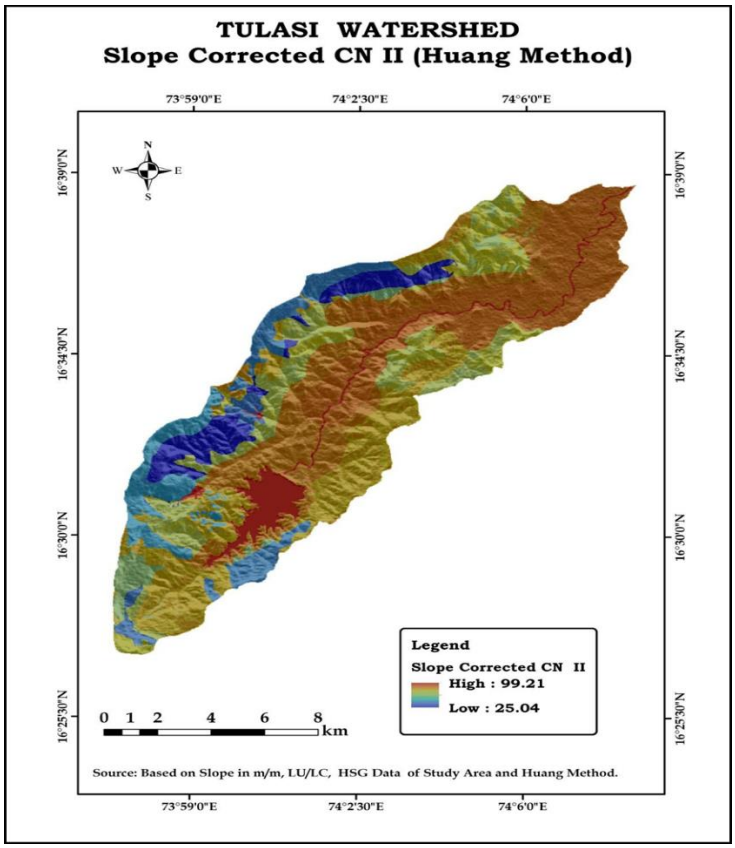

Figure 4. Slope Corrected CN II Map

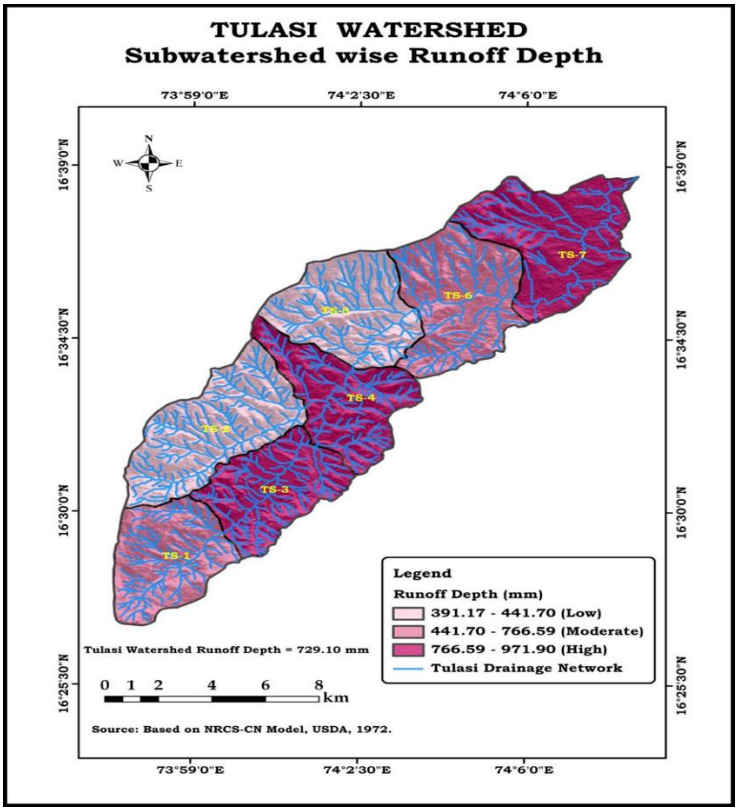

Figure 5. Subwatershed wise Runoff Depth (mm)

The runoff Curve Number (CN-II) values under average pre-existing soil moisture conditions (AMC-II) reflect the combined influence of land use–land cover and hydrological soil groups on runoff generation (Bajirao & Kumar, 2022). Highly impervious surfaces such as paved areas, parking lots, rooftops, and driveways show uniformly high CN values of 98 across all soil groups, indicating very high runoff potential. Similarly, paved streets and roads with curbs, gutters, and storm sewers also exhibit a CN value of 98 irrespective of soil type. In contrast, gravel roads display lower CN values, ranging from 76 in hydrological soil group A to 91 in group D, while earthen or dirt roads show CN values varying from 72 to 89 from group A to D. Commercial and business districts, characterized by about 85% impervious cover, record high CN values ranging from 89 in soil group A to 95 in soil group D. Industrial areas with approximately 72% imperviousness show CN values between 81 and 93 across the soil groups. Residential areas exhibit a clear decrease in CN values with increasing plot size and decreasing impervious cover. Residential plots of 1/8 acre or less show CN values ranging from 77 to 92, whereas 1-acre residential plots record lower values ranging from 51 in soil group A to 84 in soil group D.

Cultivated agricultural land shows moderate runoff potential, with CN values of 62 to 81 under conservation practices (Baghel *et al*., 2023) and higher values of 72 to 91 where conservation measures are absent. Pasture and rangeland areas demonstrate significant variation depending on vegetative condition, with good cover showing CN values from 39 to 80 and poor cover exhibiting higher values from 68 to 89. Meadow and permanent grasslands in good condition record relatively low CN values, ranging from 30 in soil group A to 78 in soil group D.

Forest areas generally exhibit lower runoff potential, particularly where dense canopy and good ground cover are present, with CN values ranging from 25 to 77 (Nageswara *et al*., 2020). However, forest areas with thin stands, poor cover, and absence of mulch show higher CN values between 45 and 83. Open spaces such as lawns, parks, cemeteries, and golf courses show moderate CN values, ranging from 49 to 84 under fair conditions and from 39 to 80 under good vegetative cover. Overall, the CN-II values highlight how increasing imperviousness and poorer soil infiltration characteristics lead to higher runoff potential under AMC-II conditions.

CONCLUSION

The surface runoff patterns observed in the study were effectively simulated using the NRCS–CN model. Critical evaluation of the model indicates that it accurately reproduces the peak flow recorded in 2013 during the monsoon season, identifying it as the maximum predicted runoff event under the current study conditions. High surface runoff potential was evident across the hill tract and the majority of the downslope areas of the upland, particularly within the middle and lower sections of the sub-watershed. Analysis of runoff potential classes revealed that medium runoff is most prevalent, especially in the upper reaches, where forest cover exhibits resilient characteristics and the soil and surface texture are predominantly coarse.

Due to the lack of a gauging station within the Tulasi watershed, direct validation of the estimated runoff values was not possible. Consequently, surface runoff calculations at the micro-watershed scale are recommended, aligned with existing water resources management practices, to enhance understanding and support effective management strategies. Moreover, combining remote sensing data with field surveys, along with GPS- and GIS-based analyses, provides accurate, standardized, and contemporary information crucial for sustainable land and water resource planning.

ACKNOWLEDGMENTS: The authors gratefully acknowledge the Geoinformatics Division, Department of Geography, Shivaji University, Kolhapur, for providing access to ArcGIS software facilities and for their valuable technical support, which substantially contributed to the successful completion of this research.

CONFLICT OF INTEREST: None

FINANCIAL SUPPORT: None

ETHICS STATEMENT: None

REFERENCES

Ali, G., Siebert, K., & Mizero, S. M. (2024). Spatiotemporal variability of runoff events in response to rainfall, snowmelt, and rain-on-snow in the Lake Erie Basin. *Journal of Hydrology: Regional Studies, 53*, 101774. doi:10.1016/j.ejrh.2024.101774

Allan, J. D., Castillo, M. M., & Capps, K. A. (2021). *Stream ecology: Structure and function of running waters*. Springer Nature. doi:10.1007/978-3-030-63814-1

Auerswald, K., & Gu, Q. L. (2021). Reassessment of the hydrologic soil group for runoff modelling. *Soil and Tillage Research, 212*, 105034. doi:10.1016/j.still.2021.105034

Baghel, S., Kothari, M., Tripathi, M. P., Das, S., Kumar, A., & Kuriqi, A. (2023). Water conservation appraisal using surface runoff estimated by an integrated SCS-CN and MCDA-AHP technique. *Journal of Earth System Science, 132*(3), 127. doi:10.1007/s12040-023-02133-x

Bajirao, T. S., & Kumar, P. (2022). Quantification of impact of spatio-temporal variability of land use/land cover on runoff generation using modified NRCS-CN method. *Arabian Journal of Geosciences, 15*(7), 610. doi:10.1007/s12517-022-09931-5

Banerjee, D., & Ganguly, S. (2023). A review on the research advances in groundwater–surface water interaction with an overview of the phenomenon. *Water, 15*(8), 1552. doi:10.3390/w15081552

Bhardwaj, A. (2019). Watershed hydrology and management. In A. Yousuf & M. Singh (Eds.), *Watershed hydrology, management and modeling* (pp. 1–17). CRC Press. doi:10.1201/9780429430633-1

Calero Mosquera, D., Hoyos Villada, F., & Torres Prieto, E. (2021). Runoff curve number (CN model) evaluation under tropical conditions. *Earth Sciences Research Journal, 25*(4), 397–404. doi:10.15446/esrj.v25n4.95321

Cao, Q., Zong, X., Qi, C., Yu, C., Guo, J., Shen, J., Wei, S., Wang, D., Zhang, J., & Xia, J. (2024). Changes in runoff and sediment

loads in the Tuhai River Basin and the factors influencing these changes. *Water, 16*(14), 2064. doi:10.3390/w16142064

Chow, V. T., Maidment, D. R., & Mays, L. W. (1988). *Applied hydrology*. McGraw-Hill.

Coppol, R., Cantile, T., Fiore, A. D., & Prisa, D. (2022). Interprofessional management of necrotizing periodontitis in an elderly patient requiring nursing care: A case report. *Asian Journal of Periodontics & Orthodontics, 2*, 106–112. doi:10.51847/7HotgYQTcU

da Silva, V. S., Salami, G., da Silva, M. I. O., Silva, E. A., Monteiro Junior, J. J., & Alba, E. (2020). Methodological evaluation of vegetation indexes in land use and land cover (LULC) classification. *Geology, Ecology, and Landscapes, 4*(2), 159–169. doi:10.1080/24749508.2019.1608409

Dharmawan, I. W. S., Pratiwi, Siregar, C. A., Narendra, B. H., Undaharta, N. K. E., Sitepu, B. S., Sukmana, A., Wiratmoko, M. D. E., Abywijaya, I. K., & Sari, N. (2023). Implementation of soil and water conservation in Indonesia and its impacts on biodiversity, hydrology, soil erosion, and microclimate. *Applied Sciences, 13*, 7648. doi:10.3390/app13137648

Doost, Z. H., Alsuwaiyan, M., & Yaseen, Z. M. (2024). Runoff management based water harvesting for better water resources sustainability: A comprehensive review. *Knowledge-Based Engineering and Sciences, 5*(1), 1–45. doi:10.1016/j.knosys.2023.107123

Eniyew, S., Meshesha, D. T., Zeleke, G. A., & Wassie, S. B. (2024). Combining geospatial information and SCS-CN for surface runoff estimation in Rib watershed, upper Blue Nile Basin, Ethiopia. *Geomatics, Natural Hazards and Risk, 15*(1), 2338533. doi:10.1080/19475705.2024.2338533

Fan, Y., Li, X., Zhang, Y., & Wang, J. (2024). The mitigating efficacy of multi-functional storage spaces in alleviating urban floods across diverse rainfall scenarios. *Sustainability, 16*(15), 6417. doi:10.3390/su16156417

Feldman, A. F., Feng, X., Felton, A. J., Konings, A. G., Knapp, A. K., Biederman, J. A., & Poulter, B. (2024). Plant responses to changing rainfall frequency and intensity. *Nature Reviews Earth & Environment, 5*(4), 276–294. doi:10.1038/s43017-024-00534-0

Hawkins, R. H., Hjelmfelt, A. T., Jr., & Zevenbergen, A. W. (1985). Runoff probability, storm depth, and curve numbers. *Journal of Irrigation and Drainage Engineering, 111*(4), 330–340. doi:10.3389/feart.2020.571477

Huang, M., Gallichand, J., Wang, Z., & Goulet, M. (2006). A modification of the Soil Conservation Service curve number method for steep slopes in the Loess Plateau of China. *Hydrological Processes, 20*(3), 579–589. doi:10.1002/hyp.5925

Jahanbani, M., Rahmati, O., Panahi, M., Lee, S., & Bui, D. T. (2024). Flood susceptibility mapping through geoinformatics and ensemble learning methods, with an emphasis on the AdaBoost-Decision Tree algorithm, in Mazandaran, Iran. *Earth Science Informatics, 17*(2), 1433–1457.

Jehanzaib, M., Ajmal, M., Achite, M., & Kim, T. W. (2022). Comprehensive review: Advancements in rainfall-runoff modelling for flood mitigation. *Climate, 10*(10), 147. doi:10.3390/cli10100147

Kaliraj, S., Chandrasekar, N., Ramachandran, K. K., & Lalitha, M. (2023). GIS based NRCS-CN modeling of rainfall-runoff in river Thamirabarani sub-basin, Southern India. *Journal of Hydro-Environment Research, 49*, 10–27. doi:10.1016/j.jher.2023.07.001

Kalogeropoulos, K., Stathopoulos, N., Psarogiannis, A., Pissias, E., Louka, P., Petropoulos, G. P., & Chalkias, C. (2020). An integrated GIS-hydro modeling methodology for surface runoff exploitation via small-scale reservoirs. *Water, 12*(11), 3182. doi:10.3390/w12113182

Kratzert, F., Klotz, D., Gauch, M., & Nearing, G. S. (2024). HESS Opinions: Never train a Long Short-Term Memory (LSTM) Network on a single basin. *Hydrology and Earth System Sciences, 28*(17), 4187–4201.

Kumar, P., Garg, V., Mittal, S., & Murthy, Y. K. (2022). GIS-based hazard and vulnerability assessment of a torrential watershed. *Environment, Development and Sustainability, 24*(1), 921–951. doi:10.1007/s10668-021-01476-z

Kumar, V., Sharma, K. V., Caloiero, T., Mehta, D. J., & Singh, K. (2023). Comprehensive overview of flood modeling approaches: A review of recent advances. *Hydrology, 10*(7), 141.

Li, M., Li, S., Liu, Q., Kang, Y., Liang, L., Yuan, X., Zhang, J., Wang, X., & Li, C. (2022). Assessment of hydrological response to multiyear drought: Insights from lag characteristics and shift magnitude. *Hydrological Processes, 36*(7), e14636. doi:10.1002/hyp.14636

Li, Y., Li, M., Liu, H., & Qin, W. (2021). Influence of soil texture on the process of subsurface drainage in saturated-unsaturated zones. *International Journal of Agricultural and Biological Engineering, 14*(1), 82–89. https://dx.doi.org/10.25165/j.ijabe.20211401.5699

Ma, R., Chen, K., Andrews, C. B., Loheide, S. P., Sawyer, A. H., Jiang, X., Briggs, M. A., Cook, P. G., Gorelick, S. M., Prommer, H., et al. (2024). Methods for quantifying interactions between groundwater and surface water. *Annual Review of Environment and Resources, 49*. doi:10.1146/annurev-environ-111522-104534

Mishra, S. K., Tyagi, J. V., & Singh, V. P. (2006). SCS-CN-based modeling of sediment yield. *Journal of Hydrology, 324*(1–4), 301–322.

Mondal, S., & Mishra, A. (2024). Quantifying the precipitation, evapotranspiration, and soil moisture network's interaction over global land surface hydrological cycle. *Water Resources Research, 60*(2), e2023WR034861. doi:10.1029/2023WR034861

Muppavarapu, N. (2023). *Water knows no geopolitical boundaries: A case study of stormwater governance and land in Jefferson County, a 120-year perspective* (Doctoral dissertation, Lamar University).

Nag, S., Roy, M. B., & Roy, P. K. (2022). Study on the functionality of land use land cover over the evaluation of groundwater potential zone: A fuzzy AHP based approach. *Journal of Earth System Science, 131*(3), 146. doi:10.1007/s12040-022-01872-7

Nageswara Rao, K. (2020). Analysis of surface runoff potential in ungauged basin using basin parameters and SCS-CN method. *Applied Water Science, 10*(1), 47. doi:10.1007/s13201-019-1129-z

Neitsch, S. L., Arnold, J. G., Kiniry, J. R., Williams, J. R., & King, K. W. (2002). *Soil and Water Assessment Tool (SWAT): Theoretical documentation, version 2000*. Texas Water Resources Institute.

NRCS. (2006). *Land resource regions and major land resource areas of the United States, the Caribbean, and the Pacific Basin*.

Pareta, K., & Pareta, U. (2012). Integrated watershed modeling and characterization using GIS and remote sensing techniques. *Indian Journal of Engineering, 1*(1), 81–91. http://www.discovery.org.in/ije.htm

Prada, A. M., Cicalău, G. I. P., & Ciavoi, G. (2024). Resin infiltration for white-spot lesion management after orthodontic treatment. *Asian Journal of Periodontics & Orthodontics, 4*, 19–23. doi:10.51847/ZTuGEanCSV

Rallison, R. E. (1980). Origin and evolution of the SCS runoff equation. In *Proceedings of the ASCE Irrigation and Drainage Symposium on Watershed Management* (Vol. II, pp. 912–924).

Ross, C. A., Ali, G. A., Spence, C., Oswald, C. J., & Phillips, A. K. (2024). Reconceptualizing threshold-mediated runoff responses: A case study from the Humber River watershed, Ontario, Canada. *Hydrological Processes, 38*(7), e15241. doi:10.1002/hyp.15241

Saber, M., Yaseen, Z. M., & El-Shafie, A. (2023). Enhancing flood risk assessment through integration of ensemble learning approaches and physical-based hydrological modeling. *Geomatics, Natural Hazards and Risk, 14*(1), 2203798. doi:10.1080/19475705.2023.2203798

Sahavacharin, A., Sompongchaiyakul, P., & Thaitakoo, D. (2022). The effects of land-based change on coastal ecosystems. *Landscape and Ecological Engineering, 18*(3), 351–366. doi:10.1007/s11355-022-00505-x

Sánchez-Murillo, R., Esquivel-Hernández, G., Birkel, C., Correa, A., Welsh, K., Durán-Quesada, A. M., Sánchez-Gutiérrez, R., & Poca, M. (2020). Tracing water sources and fluxes in a dynamic tropical environment: From observations to modeling. *Frontiers in Earth Science, 8*, 571477.

Sobhani, G. (1975). *A review of selected small watershed design methods for possible adoption to Iranian conditions* (Master's thesis, Utah State University).

Soil Conservation Department. (1972). *Handbook of hydrology*. Ministry of Agriculture, New Delhi, India.

Soil Conservation Service. (1972). *National engineering handbook: Section 4, Hydrology*. U.S. Department of Agriculture.

Tideman, E. M. (2000). *Watershed management: Guidelines for Indian conditions*. Omega Scientific Publishers.

Van Mullem, J. A. (1989). Runoff and peak discharges using Green-Ampt infiltration model. *Journal of Irrigation and Drainage Engineering, 117*(3), 354–370.

Vereecken, H., Amelung, W., Bauke, S. L., Bogena, H., Brüggemann, N., Montzka, C., Vanderborght, J., Bechtold, M., Blöschl, G., Carminati, A., et al. (2022). Soil hydrology in the Earth system. *Nature Reviews Earth & Environment, 3*(9), 573–587. doi:10.1038/s43017-022-00324-6

Xu, Y., Yu, Q., Liu, C., Li, W., Quan, L., Niu, C., Zhao, C., Luo, Q., & Hu, C. (2024). Construction of a semi-distributed hydrological model considering the combination of saturation-excess and infiltration-excess runoff space under complex substratum. *Journal of Hydrology: Regional Studies, 51*, 101642. doi:10.1016/j.ejrh.2023.101642

Yang, Y., Chen, R. S., Song, Y. X., Han, C. T., Liu, Z. W., & Liu, J. F. (2020). Spatial variability of soil hydraulic conductivity and runoff generation types in a small mountainous catchment. *Journal of Mountain Science, 17*(11), 2724–2741. doi:10.1007/s11629-020-6258-1

Zhang, J., Wang, Y., Zhang, C., & Li, D. (2022). Effect of soil thickness on rainfall infiltration and runoff generation from karst hillslopes during rainstorms. *European Journal of Soil Science, 73*(4), e13288. doi:10.1111/ejss.13288

Zhou, Y., Shao, G., & Jiang, Y. (2024). Impact of diverse rainfall patterns and their interaction on soil and water loss in a small watershed within a typical low hilly region. *Water, 16*(3), 372. doi:10.3390/w16030372